Table 1. Reproducibility, Linearity, and Sensitivity

compound	RSD (n = 8) (%) migration time	RSD (n = 8) (%) peak area	linearity correlation	detection limit (μmol/L)	improved sensitivity ratio[a]
glyoxylate	0.6	11.1	0.997	8.0	0.9
glycolate	0.6	12.4	0.997	5.2	1.7
pyruvate	0.5	8.8	0.999	9.5	0.8
lactate	0.6	5.7	0.985	2.9	1.1
fumarate	0.5	9.4	0.989	0.32	1.4
succinate	0.5	6.3	0.999	0.23	1.6
malate	0.5	4.5	0.994	0.14	4.5
2-oxoglutarate	0.5	5.3	0.985	0.73	4.9
cysteine sulfinate	0.6	6.5	0.998	0.36	4.0
PEP	0.5	5.2	0.995	0.12	3.0
DHAP	0.6	7.8	0.998	0.40	2.2
glycerophosphate	0.6	8.9	0.999	0.46	1.2
cis-aconitate	0.5	7.2	0.997	0.12	4.4
3-phosphoglycerate	0.5	4.9	0.995	0.19	2.8
isocitrate	0.5	3.6	0.996	0.19	6.0
citrate	0.5	7.3	0.988	0.09	63
gluconate	0.7	5.1	0.999	1.1	0.8
E4P	0.6	6.0	0.999	0.81	2.1
Ru5P	0.6	2.7	0.999	0.21	2.4
R5P	0.6	5.1	0.999	0.26	1.9
G1P	0.6	2.1	0.983	0.15	1.9
F6P	0.6	3.5	0.980	0.19	3.4
G6P	0.6	2.4	0.992	0.16	1.6
2,3DPG	0.5	5.8	0.997	0.13	35
6-phosphogluconate	0.5	5.4	0.999	0.18	2.9
F1,6P	0.5	5.4	0.999	0.17	3.1
AMP	0.7	3.5	0.999	0.11	2.1
IMP	0.7	4.8	0.999	0.11	2.9
GMP	0.7	3.6	0.999	0.09	2.0
NADPH[b]	0.6	4.3	0.990	0.45	2.7
CoA[b]	0.6	6.1	0.994	0.03	nc[c]
acetyl CoA[b]	0.6	5.2	0.999	0.04	5.2
malonyl CoA[b]	0.6	6.6	0.995	0.05	7.6
ADP	0.6	3.9	0.995	0.06	5.3
succinyl CoA[b]	0.6	12.1	0.996	0.15	10
GDP	0.6	5.6	0.996	0.11	5.5
UTP	0.6	3.4	0.999	0.10	7.8
ATP	0.6	5.8	0.999	0.22	6.6
GTP	0.6	14.4	0.989	0.10	15
NAD	1.1	4.8	0.999	0.11	1.8
NADH	0.7	3.4	0.999	0.49	11
NADP	0.7	6.1	0.999	0.10	2.4
FAD	0.8	10.5	0.999	0.12	2.8

[a] Improved sensitivity was calculated by dividing the detection limit with the SST316Ti stainless steel by that with the platinum needle. [b] Detected at the divalent $[M - 2H]^{2-}$ ion. [c] nc, not calculated. Improved sensitivity of CoA was not calculated because CoA was not determined by the SST316Ti stainless steel.

isopropanol aqueous solution at 80 °C for 30 min) and platinum. Metal amounts in run buffer solution in the inlet vial and separation capillary were determined using an Agilent 7500 inductivity coupled plasma mass spectrometer (Tokyo, Japan). For the capillary analysis, the polyimide coating was burned with a lighter and removed with methanol, and then the capillary was cut into five pieces (each 20 cm). Each capillary (5.4 mg) was dissolved by ultrasonic treatment in 8 mL of 38% hydrofluoric acid for 80 min, and this solution was used for the inductivity coupled plasma mass spectrometry (ICP-MS) analysis.

CE-TOFMS Conditions for Anionic Metabolite Analysis. A commercially available COSMO(+), chemically coated with a cationic polymer, capillary (50 μm i.d. × 110 cm) (Nacalai Tesque, Kyoto, Japan) was used as the separation capillary. A 50 mM ammonium acetate solution (pH 8.5) was the electrolyte for CE separation. Prior to the first use, a new capillary was flushed successively with the running electrolyte, 50 mM acetic acid (pH 3.4), and then the electrolyte again for 20 min each. Before each injection, the capillary was equilibrated for 2 min by flushing with 50 mM acetic acid (pH 3.4) and then for 5 min by flushing with the running electrolyte.[20]

A sample solution (30 nL) was injected at 50 mbar for 30 s, and −30 kV of voltage was applied. The capillary temperature was thermostated to 20 °C, and the sample tray was cooled to below 5 °C. The Agilent 1100 series pump equipped with a 1:100 splitter was used to deliver 10 μL/min of 5 mM ammonium acetate in 50% (v/v) methanol–water containing 0.1 μM Hexakis to the CE interface where it is used as a sheath liquid around the outside of the CE capillary to provide a stable electrical connection between the tip of the capillary and the grounded electrospray needle.

ESI-TOFMS was conducted in the negative ionization; the capillary voltage was set at 3500 V. For TOFMS, the fragmenter, skimmer, and Oct RFV voltage was set at 100, 50, and 200 V, respectively. A flow rate of drying nitrogen gas (heater temperature, 300 °C) was maintained at 7 L/min. Automatic recalibration

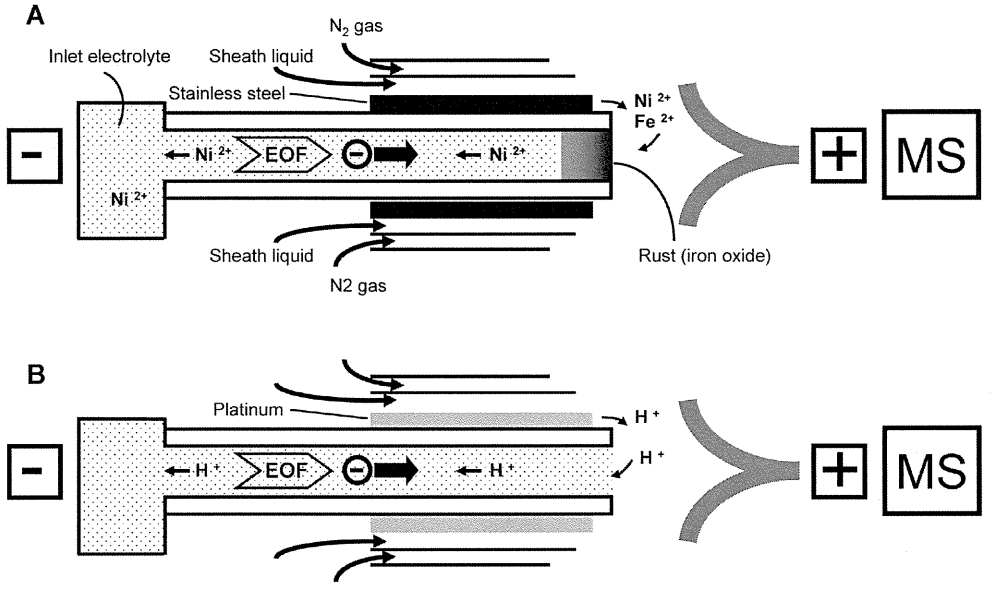

Figure 2. Schematic of anion analysis by the CE-MS in the negative mode using the CE-ESI-MS sprayer with (A) the stainless steel needle and (B) the platinum needle. (A) Metal ions like Fe^{2+} and Ni^{2+} were electrochemically generated from the stainless steel needle at the anode (pH 6.9) and moved into the separation capillary. Fe^{2+} was oxidized (forming rust) and plugged at the capillary outlet due to high electrolyte pH (8.5), while Ni^{2+} migrated toward the capillary inlet (cathode). Anions exhibiting high chelating properties with metal ions formed complexes when encountering Ni^{2+} or iron oxides. (B) In the platinum needle, water oxidation ($2H_2O \rightarrow 4H^+ + O_2\uparrow + 4e^-$) occurred at the anode and, thus, anionic metabolites did not encounter the metal ions.

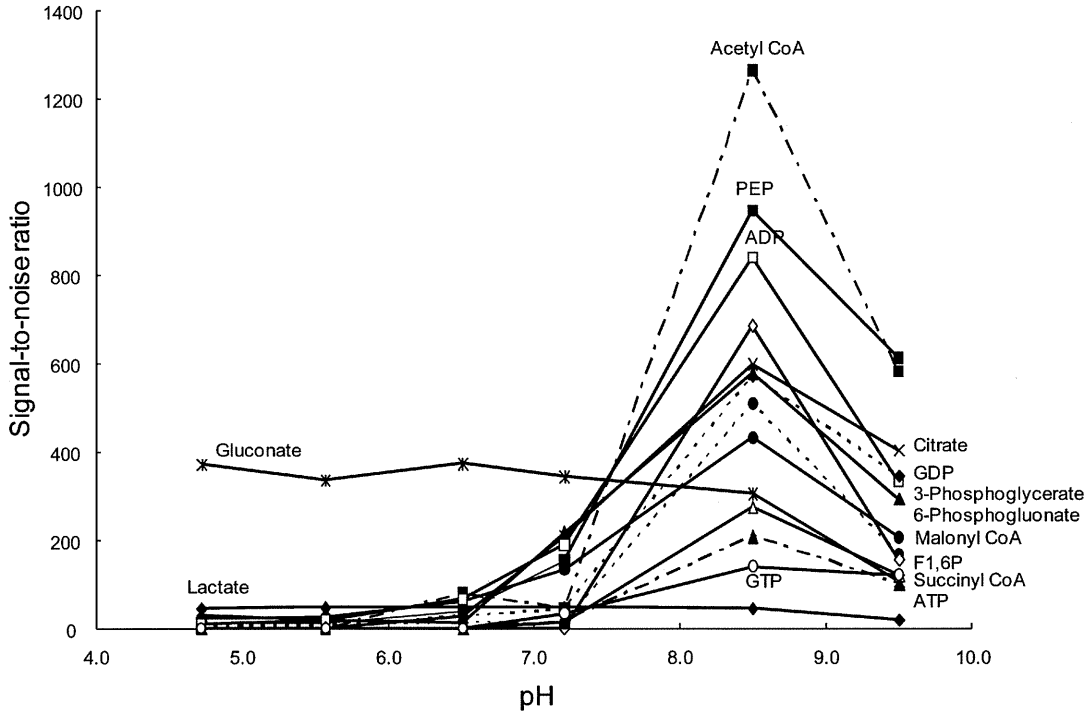

Figure 3. Effect of electrolyte pH on the sensitivity (signal-to-noise ratio) of anions. Experimental conditions: ESI spray needle, platinum; electrolyte, 50 mM ammonium acetate; other experimental conditions as in Figure 1.

of each acquired spectrum was performed using reference masses of reference standards ([^{13}C isotopic ion of deprotonated acetic acid dimer ($2CH_3COOH - H$)]$^-$, m/z 120.03841), and ([Hexakis + deprotonated acetic acid ($CH_3COOH - H$)]$^-$, m/z 680.03554). Exact mass data were acquired at a rate of 1.5 spectra/s over a 50−1000 m/z range.

Raw CE-TOFMS data were processed using software developed in-house for the quantification of metabolites.[13,25,26] All target metabolites were identified by matching their m/z values and migration times with those of standard compounds. For overall data analysis, three-dimensional representation of CE-TOFMS data was produced using MZmine2 software[27,28] (http://mzmine.sourceforge.net/).

(25) Baran, R.; Kochi, H.; Saito, N.; Suematsu, M.; Soga, T.; Nishioka, T.; Robert, M.; Tomita, M. *BMC Bioinf.* **2006**, *7*, 530.

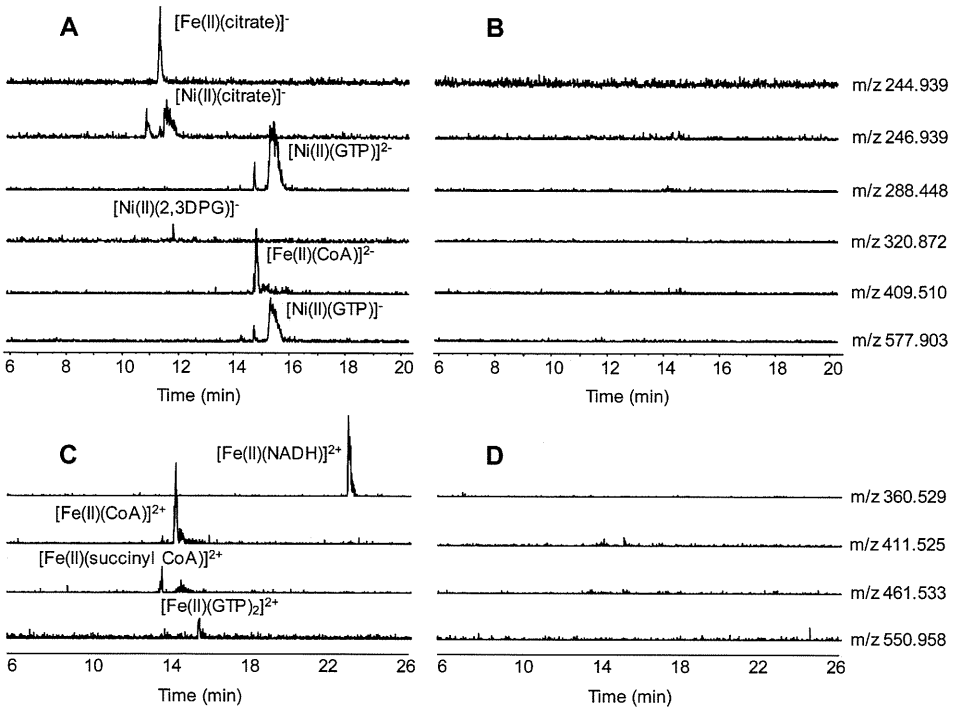

Figure 4. Abundance of metal−anion complexes in the analysis of 43 anionic metabolite standards using CE-TOFMS in the negative mode and negative ionization detection with (A) the stainless steel needle and (B) the platinum needle and positive ionization detection with (C) the stainless steel needle and (D) the platinum needle. Experimental conditions: the names of 43 anionic metabolite standards are listed in Table 1; the standard concentration was 50 μmol/L each; in the positive TOFMS detection, the ion polarity was switched to positive and the capillary voltage was set at 4000 V; other experimental conditions are the same as in Figure 1.

RESULTS AND DISCUSSION

Prevention of Capillary Plugging by Use of a Platinum ESI Needle. The sheath flow CE-MS method with negative mode using a cationic polymer-coated capillary demonstrated impressive performance for anion analysis.[13,20] However, the sensitivities of several anions were considerably poor. Moreover, migration times of every analyte immediately became longer, and the capillary frequently clogged. Removing the polyimide film, we examined a clogged capillary using a microscope and found that the capillary outlet became plugged with a rustlike precipitate. To identify it, we investigated its solubility using several organic solvents and acids including chloroform, isopropanol, acetone, acetonitrile, hydrochloric acid, hydronitric acid, and hydrosulfuric acid. Since it was only soluble in hydrochloric acid, it was identified as a transition metal having a high ionization tendency like iron and nickel.

Although the original Agilent CE-ESI-MS spray needle is made from SST316Ti stainless steel, it exhibited high ionization tendency and, thus, was oxidized to metal ions by electrolysis, resulting in a plug at the capillary outlet. To confirm this, we attached the following three types of spray needles to the Agilent ESI sprayer: normal- and passivated-SST316Ti stainless steel and platinum. Using these spray needles, we performed the CE-MS analyses with the negative mode and checked the capillary outlet with a microscope after 5, 10, and over 40 runs, respectively.

With the two needles made from the stainless steel, both the capillary outlets became plugged with precipitates (rust) after five runs and the rust grew thicker with the number of analysis performed, indicating that electrochemical oxidation of the stainless steel occurred. However, the use of the platinum needle resulted in no plugging for 100 runs. This is consistent with previous reports that platinum wire used as the CE-MS ESI electrode protects against electrode corrosion.[29−32] As Smith and Moini[31] reported, when a stainless steel wire was used as the anode, the oxidation of iron ($Fe \rightarrow Fe^{2+} + 2e^-$) (perhaps Ni, Cr, and Ti) replaced the oxidation of water ($2H_2O \rightarrow 4H^+ + O_2\uparrow + 4e^-$) by electrolysis, resulting in corrosion of the Fe and formation of Fe^{2+}. However, platinum wire only caused electrochemical oxidation of water, and bubble formation occurred at the anodic end.

The robustness of the CE-MS method with the negative mode using the SST316Ti stainless steel needle and platinum needle was further investigated. With the stainless steel needle, both capillary clogging with rust and significant corrosion at the tip of the needle occurred (Figure 1A) and the current fully dropped after 167 runs (Figure 1C). For the platinum needle, although a slight current drop and migration time fluctuation were observed (Figure 1C), it enabled over 545 successive analyses without capillary clogging and corrosion of the needle (Figure 1B). While Smith and Moini used iron wire, instead of platinum wire, as the anode to eliminate gas bubble formation in their sheathless CE-

(26) Hirayama, A.; Kami, K.; Sugimoto, M.; Sugawara, M.; Toki, N.; Onozuka, H.; Kinoshita, T.; Saito, N.; Ochiai, A.; Tomita, M.; Esumi, H.; Soga, T. *Cancer Res.* **2009**, *69*, 4918–4925.
(27) Katajamaa, M.; Oresic, M. *BMC Bioinf.* **2005**, *6*, 179.
(28) Katajamaa, M.; Miettinen, J.; Oresic, M. *Bioinformatics* **2006**, *22* (5), 634–636.
(29) Cao, P.; Moini, M. *J. Am. Soc. Mass Spectrom.* **1997**, *8*, 561–564.
(30) Herring, C. J.; Qin, J. *Rapid Commun. Mass Spectrom.* **1999**, *13*, 1–7.
(31) Smith, A. D.; Moini, M. *Anal. Chem.* **2001**, *73*, 240–246.
(32) Van Berkel, G. J.; Asano, K. G.; Schnier, P. D. *J. Am. Soc. Mass Spectrom.* **2001**, *12*, 853–862.

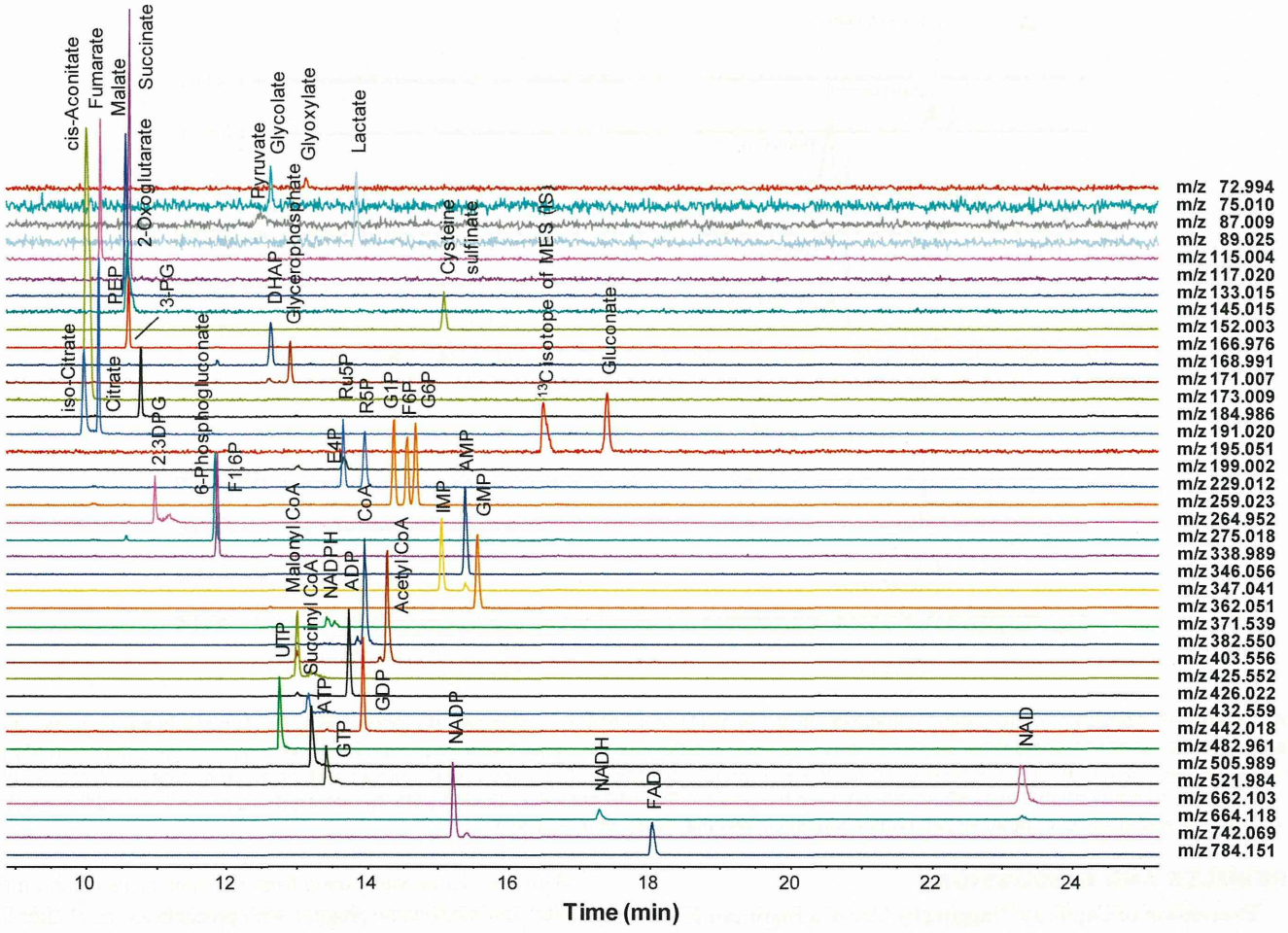

Figure 5. Selected CE-TOFMS ion electropherograms for a standard mixture of anionic metabolites in the components of glycolysis, pentose phosphate, and the TCA pathways obtained by the CE-ESI-MS sprayer attached with a platinum needle. Experimental conditions: standard concentration, 10 μmol/L each; other experimental conditions as in Figure 1. Abbreviations: PEP, phosphoenolpyruvate; DHAP, dihydroxyacetone phosphate; 3PG, 3-phosphoglycerate; E4P, erythrose 4-phosphate; Ru5P, ribulose 5-phosphate; R5P, ribose 5-phosphate; G1P, glucose 1-phosphate; F6P, fructose 6-phosphate; G6P, glucose 6-phosphate; 2,3DPG, 2,3-diphosphoglycerate; F1,6P, fructose 1,6-diphosphate; NADPH, reduced nicotinamide adenine dinucleotide phosphate; NADP, nicotinamide adenine dinucleotide phosphate; FAD, flavin adenine dinucleotide.

MS system,[31] our results indicate that bubble formation generated by the platinum needle had no effect on the analysis in the sheath flow CE-MS system.

Sensitivity Differences between the Stainless Steel Needle and the Platinum Spray Needle in Anion Analysis. There was another difficulty in analyzing anionic metabolites by the CE-MS method with the negative mode using the ESI sprayer equipped with the SST316Ti stainless steel needle. Several carboxylic acids and phosphorylated compounds such as malate, 2-oxoglutarate, 3-phosphoglycerate (3PG), citrate, isocitrate, gluconate, 2,3-diphosphoglycerate (2,3DPG), uridine 5′-triphosphate (UTP), adenosine 5′-triphosphate (ATP), guanosine 5′-triphosphate (GTP), reduced nicotinamide adenine dinucleotide (NADH), coenzyme A (CoA), and acetyl- and malonyl-CoA with a concentration below a few micromolar were not detected. However, all the anions were detected as well-defined peaks with the platinum needle.

Many carboxylic acids and nucleotides such as citrate, malate, ATP, GTP, and NADH are complexing agents,[33–38] which display high stability constants for transition metals. For phosphorylated saccharides and CoAs, stability constants for transition metals have not been frequently reported. However, as metal–phosphate affinity is well-known[33,35,39,40] and these characteristics are frequently utilized in phoshoproteomics studies,[41,42] most phosphorylated compounds will likely interact with transition metals.

Experiments show sensitivity differences between the two needles for metal-chelating carboxylic acids, and phosphorylated anions are observed (Table 1). Conversely, pyruvate, lactate, and fumarate exhibit little or no stability constants for transition metals,[34] and their sensitivities were independent of the needle type. Unlike NADH, nicotinamide adenine dinucleotide (NAD^+)

(33) Toyokuni, S. *Free Radicical Biol. Med.* **1996**, *20*, 553–566.
(34) Soga, T.; Gordon, R. A. *J. Chromatigr., A* **1997**, *767*, 223–230.
(35) Kowaltowski, A. J.; Vercesi, A. E. *Free Radical Biol. Med.* **1999**, *26*, 463–471.
(36) Canaviri, E. C.; Feliz, M. R.; Capparelli, A. L. *Transition Met. Chem.* **1992**, *17*, 446–448.
(37) Champeil, P.; Rigaud, J. L.; Gary-Bobo, C. M. *Proc. Natl. Acad. Sci. U.S.A.* **1980**, *77*, 2405–2409.
(38) Lvovich, V.; Scheeline, A. *Arch. Biochem. Biophys.* **1995**, *320*, 1–13.
(39) Takebayashi, Y.; Mitsuma, R.; Imanari, T. *Anal. Sci.* **1987**, *3*, 569–572.
(40) Ziemniak, S. E.; Jones, M. E.; Combs, K. E. S. *J. Solution Chem.* **1989**, *18*, 1133–1152.
(41) Stensballe, A.; Andersen, S.; Jensen, O. N. *Proteomics* **2001**, *1*, 207–222.
(42) Kokubu, M.; Ishihama, Y.; Sato, T.; Nagasu, T.; Oda, Y. *Anal. Chem.* **2005**, *77*, 5144–5154.

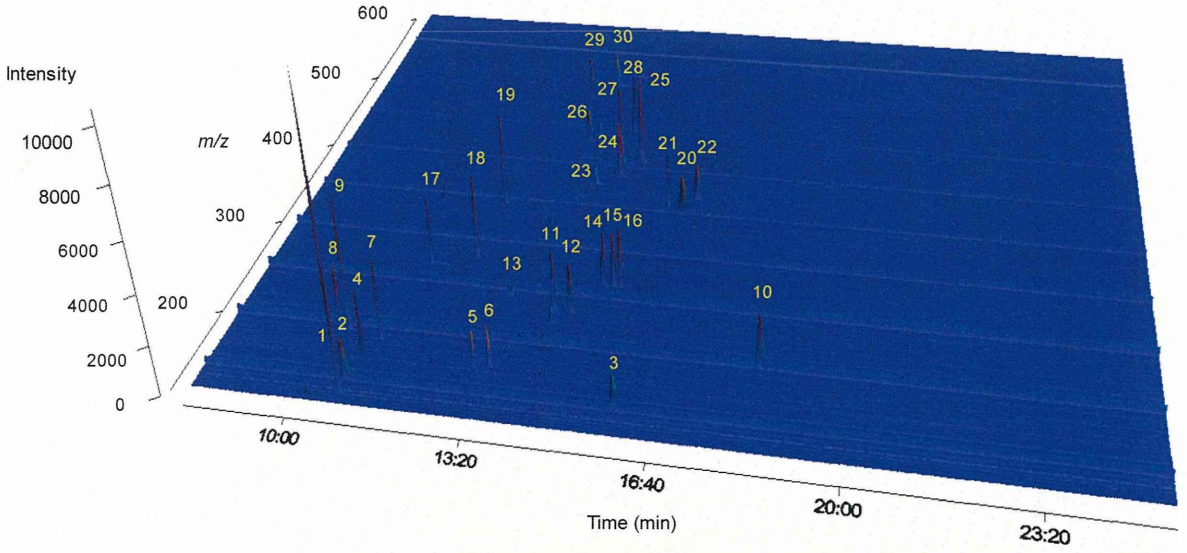

Figure 6. Three-dimensional representation (total ion electropherogram) for the analysis of a standard mixture of anionic metabolites found in glycolysis, pentose phosphate, and the TCA pathways. Results were obtained by the CE-TOFMS in the negative mode using the CE-ESI sprayer with a platinum needle. Experimental conditions: standard concentration, 50 μmol/L each; other experimental conditions are the same as in Figure 1. Peaks: 1, malate; 2, 2-oxoglutarate; 3, cysteine sulfinate; 4, PEP; 5, DHAP; 6, glycerophosphate; 7, 3PG; 8, isocitrate; 9, citrate; 10, gluconate; 11, E4P; 12, Ru5P; 13, R5P; 14, G1P; 15, F6P; 16, G6P; 17, 2,3DPG; 18, 6-phosphogluconate; 19, F1,6P; 20, AMP; 21, IMP; 22, GMP; 23, NADPH; 24, CoA; 25, acetyl CoA; 26, malonyl CoA; 27, ADP; 28, GDP; 29, UTP; 30, ATP.

does not form a complex with the Fe^{2+} ion;[38] thereby, NAD^+'s sensitivity is most similar between the two needles. These facts indicate that the anions' metal-chelating properties likely affect their detection sensitivities.

Effect of Generated Metal Ions on Sensitivity in Measurement of Anionic Metabolites. To investigate the hypothesis that anionic metabolites exhibiting high stability constants for metal ions might form complexes with the iron oxides generated by the stainless steel needle, the separation capillary was cut into five pieces (each 20 cm) and analyzed by ICP-MS. The ICP-MS analysis detected a 10.4 ppb level of Fe in the tip of the capillary outlet (the anode side), which identified the rust as iron oxide, but no metals in other regions of the capillary. Surprisingly, nickel was detected in the capillary inlet electrolyte, and its concentration dramatically increased (0.96 μg/L at 1 h and reached 3.08 μg/L at 2 h) even when no sample was injected. This indicates that nickel ion migrated from the anode to the inlet electrolyte vial. However, no such phenomena were observed when using the platinum needle.

It is, therefore, assumed that, with the stainless steel needle (Figure 2A), iron and nickel ions generated at the anode due to electrolysis moved to the capillary outlet in the sheath liquid (pH 6.9) and iron oxides formed because of the high pH (pH 8.5)[20] (Figure 3). Simultaneously, Ni^{2+} ions migrated toward the cathode without precipitation and then collected in the capillary inlet electrolyte vial. In this manner, injected anionic metabolites encountered Ni^{2+} in the separation capillary or the iron oxides at the capillary end and formed metal–anion complexes (Figure 2A). In the case of the platinum needle, water oxidation ($2H_2O \rightarrow 4H^+ + O_2\uparrow + 4e^-$) occurred at the anode due to its low ionization tendency and anionic metabolites did not encounter the metal ions and were fully detected by the mass spectrometer (Figure 2B).

The formation of metal–anion complexes during the CE-MS analysis was also confirmed. As listed in Table 1, when the stainless steel needle was used, a significant drop in sensitivity was observed for many anions including citrate, 2,3DPG, GTP, CoA, succinyl CoA, and NADH. For these anions, the formation of all nickel(II)– and iron(II)–anion complexes was analyzed by the CE-TOFMS method. In the negative ionization TOFMS method, nickel(II)– and iron(II)–anion complexes such as $[Fe(II)-(citrate)]^-$, $[Ni(II)-(citrate)]^-$, $[Ni(II)-(GTP)]^{2-}$, $[Ni(II)-(2,3DPG)]^-$, $[Fe(II)-(CoA)]^{2-}$, and $[Ni(II)-(GTP)]^-$ were detected with the stainless steel needle (Figure 4A). Moreover, positively charged nickel(II)– and iron(II)–anion complexes such as $[Fe(II)-(NADH)]^{2+}$, $[Fe(II)-(CoA)]^{2+}$, $[Fe(II)-(succinyl\ CoA)]^{2+}$, and $[Fe(II)-(GTP)_2]^{2+}$ were present in the positive ionization TOFMS detection (Figure 4C). These results indicate that all the anions formed complexes with nickel(II) and iron(II) ions with the stainless steel needle. No metal complexes were observed with the platinum needle (Figure 4B,D).

It was found, however, that the sensitivities for pyruvate, lactate, and fumarate were equivalent using either the stainless steel or platinum needle (Table 1). Although a trace of $[Fe(II)-(pyruvate)_3]^-$ was detected with the stainless steel needle, neither these nickel(II)– nor iron(II)–anion complexes were detected with either needle. These results indicate that with the stainless steel needle, anions exhibiting high stability constants with metals formed complexes with nickel and iron ions generated by electrolysis, resulting in a significant decrease in detection sensitivity.

Effect of Electrolyte pH on Rust Formation and Sensitivity in the CE-MS System. Given that iron ions generated from the stainless steel needle precipitated when encountering the alkaline electrolyte (pH 8.5), they are expected to be dissolved under acidic conditions. To confirm this, iron oxide formation was studied over

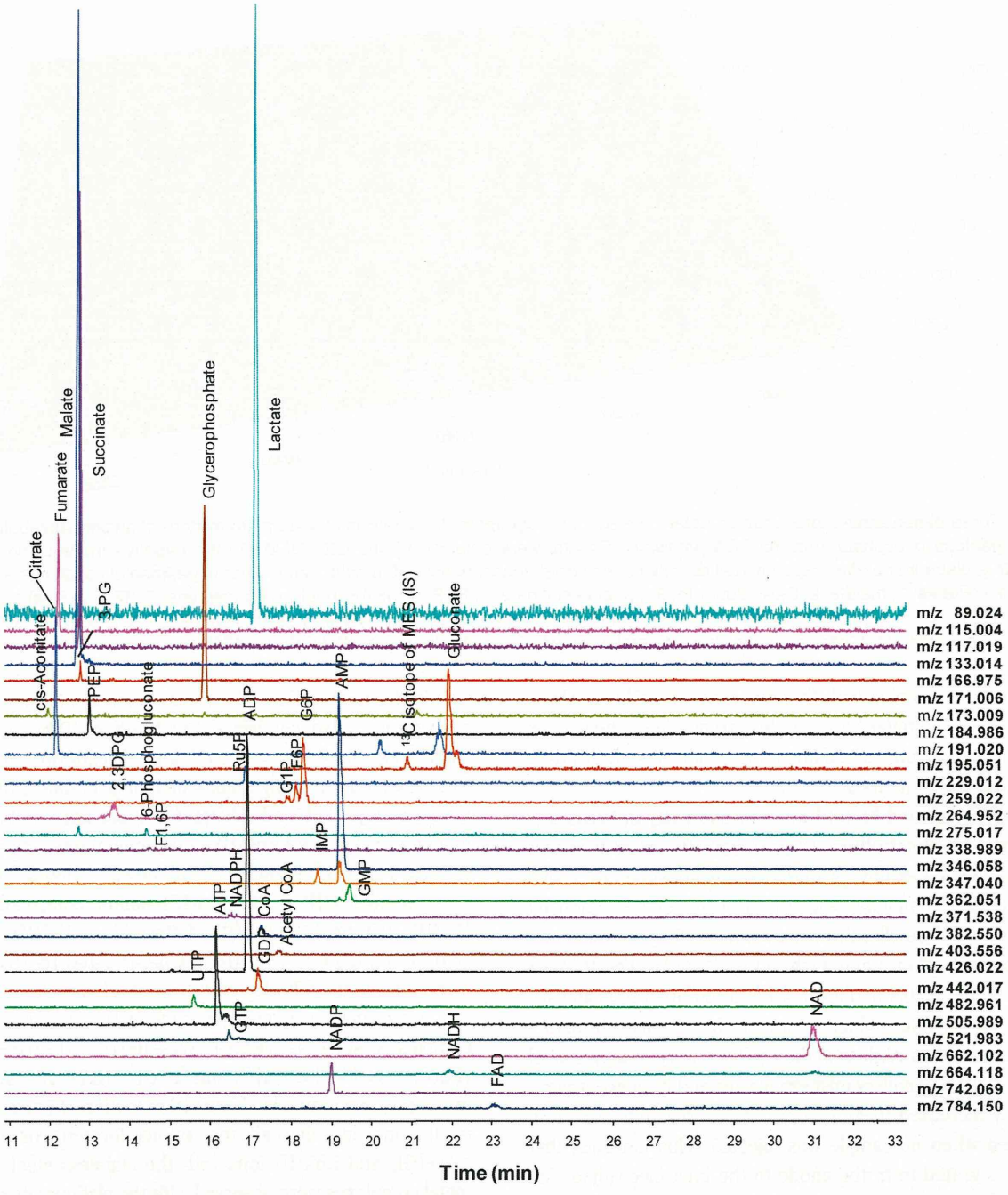

Figure 7. Selected CE-TOFMS ion electropherograms for components of glycolysis, pentose phosphate, and the TCA pathways in mouse liver. Experimental conditions are the same as in Figure 1.

pH range 4.7−9.5 using 50 mM ammonium acetate as the electrolyte and the stainless steel needle. At a pH value of 7.5, both rust development at the capillary end and corrosion of the stainless steel needle were observed. At pH 5.0, although corrosion of the needle was still observed, no iron oxide was formed. After the voltage was applied (no sample injection) for 2 h at the pH 5.0, metals at the capillary inlet electrolyte were analyzed by ICP-MS. Fe, Ni, and Ti, some components of the SST316Ti stainless steel, were detected at amounts of 1.23, 0.88, and 0.24 μg/L, respectively, which strongly implies that these metal ions were generated by electrolysis and migrated toward the cathodes.

Nevertheless, decreasing electrolyte pH had a significant effect on the detection sensitivity of anionic species (Figure 3). Below pH 7.5, although the reason was unclear, a considerable deterioration in the peak shape and extended migration time of many anions including phosphorylated substrates, nucleotide di- and triphosphates, and CoAs were observed, which resulted in substantial reduction in their detection sensitivity. Particularly, neither nucleotide triphosphates nor CoAs were detected below pH 6.5. Sensitivities of anions also decreased when the pH was increased to pH 9.5. Maximal sensitivities for most anions were obtained at pH 8.5 (Figure 3). This result was independent of the ESI needle type used. Reduction of sensitivity depending on the pH may be caused by the interaction between these compounds and the cationic coated polymer on the capillary wall, though further investigation is necessary.

In conclusion, there is no pH that can be used with the stainless steel needle to both prevent iron oxide formation and maintain

Table 2. Metabolite Amount, Reproducibility, and Recovery in Mouse Liver Analysis

compound	amount (nmol/g)	RSD (n = 12) (%)	recovery rate (average, n = 5) (%)
glyoxylate	nd[a]		106
glycolate	nd		117
pyruvate	nd		138
lactate	2440	5.7	67
fumarate	247	8.4	99
succinate	526	4.9	65
malate	1250	2.6	53
2-oxoglutarate	nd		94
cysteine sulfinate	nd		101
PEP	44	7.8	96
DHAP	nd		100
glycerophosphate	1310	3.9	97
cis-aconitate	6.0	15.6	141
3-phosphoglycerate	159	5.0	103
isocitrate	nd		103
citrate	264	6.1	89
gluconate	675	4.5	109
E4P	nd		114
Ru5P	68	11.1	101
R5P	nd		98
G1P	34	12.7	97
F6P	98	7.0	92
G6P	392	4.7	95
2,3DPG	215	5.1	93
6-phosphogluconate	23	21.9	97
F1,6P	22	15.8	92
AMP	1240	2.1	96
IMP	81	7.9	98
GMP	143	4.8	93
NADPH (divalent)	66	16.5	146
CoA (divalent)	68	10.0	132
acetyl CoA (divalent)	14	15.4	96
malonyl CoA (divalent)	nd		110
ADP	1500	4.7	88
succinyl CoA (divalent)	nd[a]		58
GDP	181	3.0	94
UTP	89	15.3	94
ATP	889	3.8	120
GTP	149	6.2	183
NAD	494	3.7	93
NADH	166	7.2	114
NADP	184	4.9	90
FAD	47	7.5	92

[a] nd, not detected.

peak shape for necessary detection sensitivity. For the platinum needle, pH 8.5 was found optimal.

Method Validation. Figure 5 illustrates selected ion electropherograms of the 43 anionic metabolite standards in the components of glycolysis, pentose phosphate, and the tricarboxylic acid (TCA) pathways obtained by the sheath flow CE-TOFMS with the negative mode using the platinum spray needle. A three-dimensional presentation (total ion electropherogram) is shown in Figure 6. This analysis will be particularly important to analyze unknown metabolites. This approach provided much better sensitivity and, thereby, contributed to excellent performance, compared to the previous method. Most of compounds were detected at their monovalent deprotonated molecular $[M - H]^-$ ions, while intensity in the divalent $[M - 2H]^{2-}$ ion of NADPH and CoA compounds was higher than that in monovalent ion.

The reproducibility, linearity, and sensitivity of this method are listed in Table 1. Practical reproducibility was obtained for all anionic species with relative standard deviation (RSD) values (n = 8) for migration times between 0.5 and 1.1% and for peak areas better than 10% except for glyoxylate, glycolate, succinyl CoA, GTP, and FAD, as indicated in the table. The calibration curves for all species were linear at 1, 2, 5, 10, 20, 50, 100, and 200 μmol/L with correlation coefficients between 0.980 and 0.999.

This method significantly improved the sensitivity of many anions. Although the previous method using the stainless steel needle was unable to detect 20 μmol/L of CoA, the use of the platinum needle dramatically improved sensitivity and enabled the detection of 1 μmol/L of CoA. Moreover, the sensitivities for the anions exhibiting high stability constants for metal ions such as citrate, 2,3DPG, GTP, and NADH were 63-, 35-, 15-, and 11-fold superior to those obtained by the stainless steel needle, respectively. Also several-fold better sensitivities for many anions including malate, 2-oxoglutarate, *cis*-aconitate, isocitrate, ADP, ATP, GDP, UTP, and succinyl-, acetyl-, and malonyl CoA were obtained.

Anions exhibiting low stability constants with metals such as pyruvate and lactate showed similar sensitivities between the two needles. Overall, the concentration detection limits for most of the anions, except for glyoxylate, glycolate, pyruvate, and lactate, were between 0.03 and 1.1 μmol/L with a pressure injection of 50 mbar for 30 s (30 nL); i.e., mass detection limits ranged from 0.8 to 33 fmol, at a signal-to-noise ratio of 3.

Analysis of Mouse Liver Metabolites in the Central Carbon and Energy Metabolism. The utility of the CE-TOFMS method was demonstrated by the simultaneous analysis of the central carbon and energy metabolism components extracted from mouse liver. There are more than 40 anionic intermediates that belong to several categories of chemical compounds: phosphorylated saccharides, phosphorylated carboxylic acids, carboxylic acids, nucleotides, and cofactors. Simultaneous, quantitative, and direct analysis of these compounds is a challenging analytical problem. Figure 7 shows the results for the analysis of the central carbon and energy metabolic components extracted from mouse livers obtained by the CE-TOFMS method. The 32 components were identified by comparing their molecular weights and migration times with those of metabolite standards, and their amounts were quantified by their standard calibration curves (Table 1). The relative standard deviations (n = 12) for the amounts of identified compounds in the mouse liver sample were better than 6% except for small compounds. To investigate quantification accuracy and ion suppression effect in this system, we analyzed mouse liver samples spiked with 20 μM of each standard and calculated the recovery (Table 2). Except for a few metabolites, the recovery rates of most metabolites in the CE-TOFMS approach were between 80 and 130%. Although the reason was not clear, the recovery rate of GTP was unusually high (183%). Considering the good reproducibility and recovery rates, the CE-TOFMS method in the negative mode using the platinum spray needle seems to be scarcely affected by the ion suppression effect and it enables sufficient quantitative analysis of most anionic intermediates in the central carbon and energy metabolic pathways extracted from mouse liver samples.

CONCLUSIONS

A negatively charged metabolites profiling approach based on sheath flow CE-TOFMS with a negative mode is described. The material of the ESI spray needle had a significant effect

on the measurement of anions. Due to electrolysis, the stainless steel sprayer needle was easily oxidized and generated metal ions, which caused corrosion of the needle and capillary clogging. Moreover, metal ions formed complexes with many anions, significantly decreasing detection sensitivity. The key to success was using a platinum spray needle, a low ionization tendency metal, which prevented both generation of metal ions and corrosion of the needle caused by electrolysis. Compared with the previously reported techniques, this method has several advantages: (1) it is able to integrate two CE-MS methods into one method, and thereby, all types of anionic components such as phosphorylated saccharides, phosphorylated carboxylic acids, carboxylic acids, CoA compounds, nucleotides, and nicotinamide adenine dinucleotides are simultaneously analyzed; (2) more than several-fold increased sensitivities of anions which exhibit high metal chelating properties are obtained; and (3) the present method provides improved reproducibility, quantification accuracy, and method robustness (i.e., capillary lifetime). Its utility was demonstrated by the simultaneous and quantitative analysis of the central carbon and the energy the metabolic intermediates extracted from mouse livers. These results indicate that the proposed CE-TOFMS method can be useful for the comprehensive analysis of anionic species in a wide range of application areas.

ACKNOWLEDGMENT

We thank Akiyoshi Hirayama and Dr. Masahiro Sugimoto, Institute for Advanced Biosciences, Keio University, and Takamasa Ishikawa, Human Metabolome Technologies Inc., for technical support, and Dr. David N. Heiger, Agilent Technologies, for critical reading of the manuscript. This work was supported in part by grants for the Health and Labour Sciences Research Grants entitled "Research on Risk of Chemical Substances" and "Research on Biological Markers for Drug development", by a Grant-in-Aid for Creative Scientific Research 17GS0419 from the Japan Society for the Promotion of Science, by a grant from the Global COE Program entitled "Human Metabolic System Biology", and by a Grant-in-Aid for Scientific Research on Priority Areas "Life surveyor" and "Systems Genomes" from the Ministry of Education, Culture, Sport, Science, and Technology (MEXT) in Japan as well as by research funds from Yamagata prefectural government and Tsuruoka city.

Received for review March 31, 2009. Accepted May 31, 2009.

AC900675K

はじめに
Introduction

曽我朋義
Tomoyoshi SOGA
慶應義塾大学先端生命科学研究所

トランスクリプトミクス，プロテオミクス，メタボロミクス等のオミクス研究は細胞や生体内の多数の構成成分の変化をバイアスをかけない手法により網羅的に探索し，生命現象を包括的に理解しようとするものである．従来の仮説検証型の科学に対して，オミクスは網羅的なデータ解析によって背後に隠れている因子をみつけ出そうとする仮説発見型研究であり，だれも予想もしていなかった大発見をもたらす可能性を秘める．

今回はポストゲノム医学の新しい研究手法として最近注目を集めているメタボロミクスについて特集した．生物の活動は代謝とよばれるさまざまな酵素による化学反応の連鎖によって支えられている．代謝のおもな役割は外界から取り入れた物質をエネルギー(ATP)や，DNA，蛋白質などの生体高分子の前駆体(ヌクレオチド，アミノ酸など)あるいは脂質などに変換することである．代謝によって生産された代謝中間体や代謝産物の総称をメタボロームとよび，微生物で数百，哺乳動物で数千，植物で数万種類の代謝産物が存在するといわれている．

代謝物質は，物理的化学的性質が非常に似かよったものから，まったく異なるものまで数百種から数万種類存在するため，ひとつの分析法ですべてのメタボロームを測定することはいまだ困難である．しかし，ガスクロマトグラフィ-質量分析計(GC/MS)，高速液体クロマトグラフィ-質量分析計(LC-MS)，キャピラリー電気泳動-質量分析計(CE-MS)など定量的なメタボローム測定法が確立され，近年急速にメタボロミクスが医薬分野の基礎から応用研究に用いられるようになった．通常，代謝は高度に調節され，安定化されているが，代謝の異常で多くの疾患が引き起こされることや，癌細胞が異常な代謝を示すことなどは広く知られており，癌や疾病の機序解明や創薬開発には包括的に代謝を理解することが必要である．

本特集では，医薬分野で興味深いメタボローム解析を展開されている研究者に最新の成果を簡単に紹介していただいた．メタボロミクスはまだ生まれたばかりの方法論である．意欲的な人材がこの研究分野に参画し，新天地を切り開いてくれることを期待したい．

ヒト癌組織のメタボローム解析

Metabolome analysis of human tumor tissues

平山明由(写真)　曽我朋義
Akiyoshi HIRAYAMA and Tomoyoshi SOGA
慶應義塾大学先端生命科学研究所メタボローム解析グループ

◎キャピラリー電気泳動-質量分析装置(CE-MS)を用いたメタボローム測定法は，各種サンプル中に含まれるイオン性低分子代謝物の網羅的測定に適している．とくに解糖系，ペントースリン酸回路，TCA 回路をはじめとして，アミノ酸代謝やプリン，ピリミジン代謝など，エネルギー代謝に関与する代謝物のほとんどはイオン性であることから，本法はエネルギー代謝を解明するうえで有用なツールになると考えられる．本稿ではCE-MS によるメタボローム解析を用いて，癌の微小環境における特殊なエネルギー代謝を明らかにした研究成果を紹介したい．

Key word：キャピラリー電気泳動-質量分析装置(CE-MS)，ワーバーグ効果，フマル酸呼吸

癌は周知のとおり，増殖，浸潤，転移を繰り返し，結果的にヒトを死に至らしめる疾患であるが，これまでに癌組織のエネルギー代謝を包括的に調べた研究例はほとんどない．通常，癌が増殖するためには膨大なエネルギー(ATP)が必要になるはずであるが，これら必要なエネルギーがどのように産生され，供給されているのかについては未知の部分も多い．メタボロームは生体内の代謝産物の総体を示す用語であるが，著者らはこれまでに，おもにキャピラリー電気泳動-質量分析装置(capillary electrophoresis-mass spectrometer：CE-MS)を用いたメタボローム解析を，微生物[1,2]，植物[3]，動物[4]などのサンプルに適用してきた．CE-MS は解糖系，ペントースリン酸回路，TCA 回路をはじめとして，アミノ酸代謝，プリン代謝やピリミジン代謝などのエネルギー代謝に必須な代謝物群の一斉定量に有用な測定法である(「サイドメモ」参照)．

本稿では，CE-MS を用いたメタボローム解析を癌の微小環境における代謝の解明に応用し，得られた成果[5]を紹介する．

低酸素と癌のエネルギー代謝

癌細胞が好気的条件下においてもミトコンドリアでの呼吸を使わずに，おもに解糖系によってエネルギー産生を行う現象はワーバーグ効果[6]とよばれ，これまでにさまざまな癌種において確認されている．癌には，肝癌や胃癌のように比較的酸素分圧の高い癌と，膵癌や大腸癌のように癌細胞のまわりに血管がほとんどない(酸素分圧の低い)タイプの癌が存在し，一般的には後者のほうが増殖能力は高いといわれている．癌が増殖するには

サイドメモ　CE-MS

キャピラリー電気泳動(capillary electrophoresis：CE)と質量分析装置(mass spectrometer：MS)を並列につないだ分析装置の略称．内径数十 μm のキャピラリー(毛細管)の中に泳動液を満たし，両端に数十 kV の高電圧を印加することによって，キャピラリー内の物質をその電荷と水和イオン半径に基づいて分離した後，質量分析装置に導入することによって，高分離・高感度に検出する分析手法である．

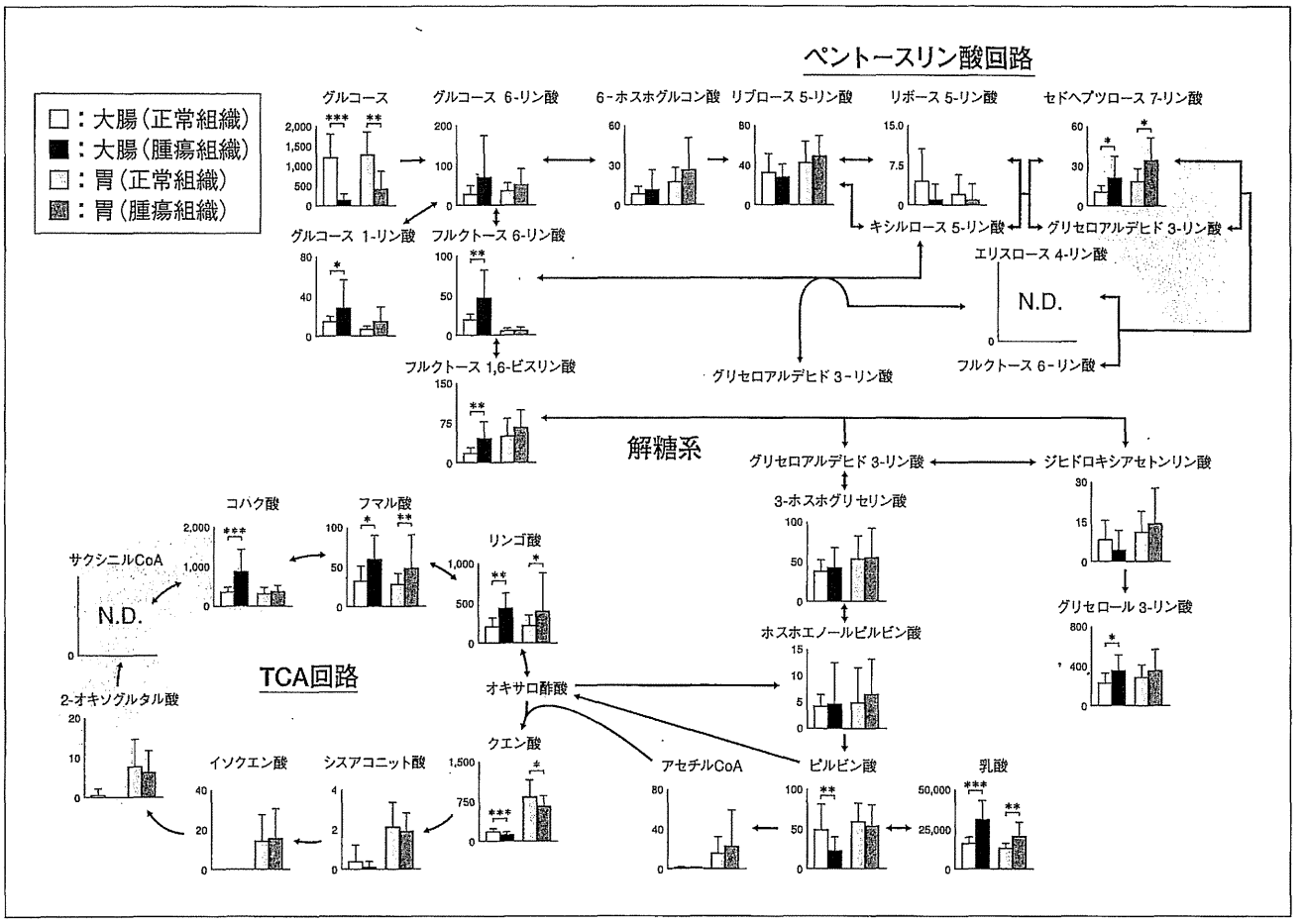

図 1　解糖系，ペントースリン酸回路，TCA回路に関与する代謝物の変動[5)]

各代謝物量は1g臓器当りの平均値±標準偏差で示してある．また，統計学的有意差の算出にはWilcoxon検定を用いた．
*：$p<0.05$，**：$p<0.01$，***：$p<0.001$．

エネルギーとしてのATPが必要不可欠であるが，大部分のATPは解糖系か酸化的リン酸化によって生産される．しかし，血管がないところで増殖する癌細胞は，解糖系に必要なグルコース量も酸化的リン酸化で必要な酸素も不足している．血流不足によって解糖系も酸化的リン酸化も制限された環境下においても増殖を続けられる癌細胞は，いったいそのエネルギーをどのように産生しているのであろうか．

そこで著者らは，キャピラリー電気泳動-飛行時間型質量分析装置(CE-TOFMS)を用いたメタボローム測定により，大腸癌および胃癌患者から採取した腫瘍組織および正常組織の代謝物質を一斉分析し，癌組織におけるエネルギー代謝のメカニズムの解明を試みた．

中心炭素代謝

今回，著者らはCE-TOFMSを用いたメタボローム測定によって，16名の大腸癌患者，および12名の胃癌患者の腫瘍組織中から，約800～1,100種類の代謝物質由来と思われるピークを得た．そのうち，エネルギー代謝にとくに重要である解糖系，ペントースリン酸回路，TCA回路の代謝中間体を代謝経路上にマッピングした結果を図1に示す．これらの代謝物に関しては標準物質を用いて各臓器1g中の定量値を算出し，全サンプルの平均値をグラフに記載した．なお，グルコースに関しては液体クロマトグラフ-質量分析装置(LC-MS)を用いて定量値を算出した．

まず，腫瘍組織中のグルコース量はその正常組織中の量と比較して，大腸癌で約1/10，胃癌では約1/3程度であった．さらに，これらは血中グルコース濃度と比較するとわずか1/45(大腸癌)～1/13(胃癌)にしかならなかった(組織密度を1g/ml，血中グルコース濃度を1mg/mlと仮定した場合)．このことは生体内の癌が，最初に予想したと

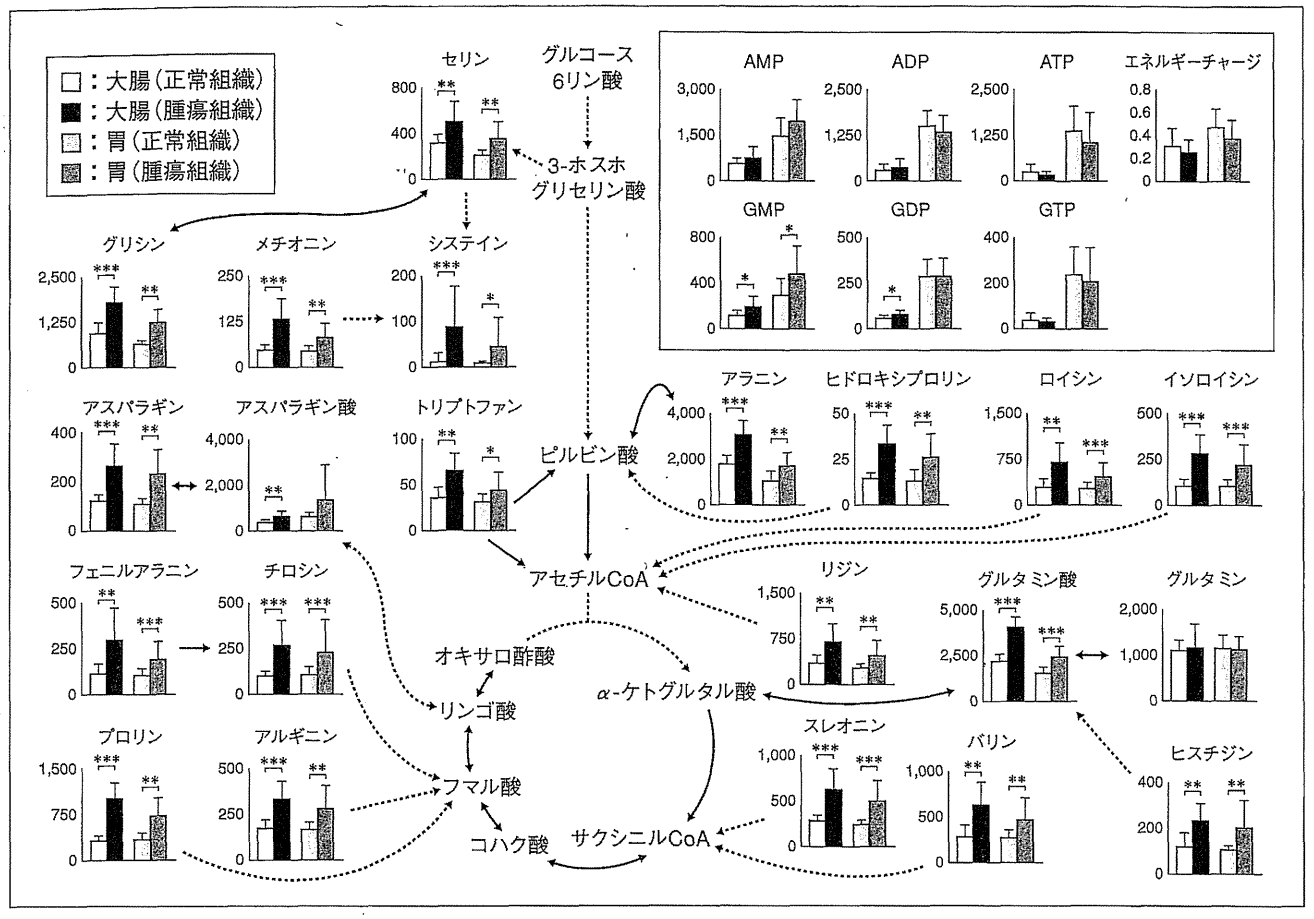

図 2　アミノ酸，ヒドロキシプロリン，ヌクレオチド類およびエネルギーチャージの変動[5]
各グラフの表示は図 1 と同じ．

おり血流の乏しい劣悪な環境下に存在していることを示唆している．一方で，解糖系の中間体物質量は非腫瘍組織と比べて同等かそれ以上であり，さらに解糖系の最終産物である乳酸量は両腫瘍組織において有意に高かった．このことから，Warburg が報告したように実際のヒトの腫瘍組織でも解糖系が亢進していることが明らかになった．

つぎに TCA 回路の代謝物に目を向けると，胃では正常，腫瘍組織とも TCA 回路の代謝中間体は一定量存在していたが，大腸では正常・腫瘍組織とも TCA 回路前半の代謝物(クエン酸からサクシニル CoA まで)がほとんど検出されておらず，ATP 量もきわめて低かった．大腸の酸素分圧は，胃のそれに比べて 1/5 程度という報告もあることから，おそらく大腸では正常組織も腫瘍組織も酸化的リン酸化反応はほとんど行われていないのではないかと推測される．

一方，TCA 回路後半の代謝物については癌特異的な傾向がみられた．とくに大腸の腫瘍組織において，TCA 回路の後半部分の代謝物(コハク酸，フマル酸，リンゴ酸)が有意に増加していた．この原因は謎であったが，寄生虫の呼吸にこの謎を解くヒントがあった．古くから嫌気性微生物や回虫などの寄生虫や二枚貝の一部では，嫌気的条件下でフマル酸呼吸とよばれる代謝によって ATP 産生が行われることが知られていた[7,8]．フマル酸呼吸は，電子伝達系における電子受容体として酸素の代りにフマル酸を用いて嫌気的に ATP を生成する反応であるが，その際に副生成物としてコハク酸を生じる．今回得られた大腸癌組織の結果においてもコハク酸が多く蓄積しており，嫌気的条件下での回虫の代謝パターンと類似していた．

一方，ある種の虫下し薬はフマル酸呼吸を阻害することが報告されており，著者らは虫下し薬を膵癌の培養細胞に添加すると癌細胞が死滅することをすでに実験で確かめている．これらを勘案した結果，現在のところ著者らは癌細胞もフマル酸呼吸かそれに類似した代謝によって ATP を産生

しているのではないかと考えている．

アミノ酸とヌクレオチド

図1に示したように，癌細胞では血流不足に伴い供給されるグルコース量も不足している．腫瘍組織はATP産生の一部をフマル酸呼吸に頼るとしても，それに必要なフマル酸はどこから供給されるのであろうか．図2に大腸および胃癌患者の正常，腫瘍組織のアミノ酸およびヌクレオチド量を示した．どちらの癌種においてもグルタミン以外のすべてのアミノ酸が有意に増加していた．血管新生が不十分な癌組織ではグルコース同様，血液からのアミノ酸の供給も不足していると考えられるため，これらのアミノ酸の増加は不思議である．

著者らは，必須アミノ酸も増加していること，ならびにコラーゲンの分解によって特異的に生成されることが知られているヒドロキシプロリン[9]量が増加していることから，腫瘍組織ではオートファージ[10,11]を活性化させることによりコラーゲンなどの周囲の蛋白質を積極的に分解し，ATPを生産するための前駆体としてアミノ酸を取り入れているのではないかと考えている．正常組織と腫瘍組織で唯一差のみられなかったグルタミンについては，グルタミノリシスという特殊な代謝がさまざまな癌種において活性化されている[12,13]ことがすでに知られている．つまり，癌細胞においてはグルタミンを特異的に消費する代謝経路が亢進しているために両組織間の差がなくなったものと考えられる．

最後に，大腸癌および胃癌の各組織におけるエネルギーチャージ[14]を比較した．興味深いことに，部分的にはまったく異なったエネルギー産生を行っているように思えたが，全体としてのエネルギーバランスは一定に保たれていることが証明された．

おわりに

本稿ではCE-MSを用いたメタボローム解析について，癌組織のエネルギー代謝の解明に応用した例をあげて紹介した．イオン性代謝物の一斉分析を可能にするCE-MSを用いて，著者らはすでに代謝調節メカニズムの解明，新規代謝経路の探索や各種バイオマーカーの探索など，基礎から応用に至るまでのさまざまなプロジェクトを推進し，成果を得つつある．本稿がCE-MSをはじめとしたメタボローム解析を理解していただく助けになれば幸いである．

謝辞：サンプル提供ならびにデータ解析に関してサポートをいただいた，国立がんセンター東病院の江角浩安病院長，小野塚博子博士，木下　平博士，斎藤典男博士，落合淳志博士，ならびに慶應義塾大学先端生命科学研究所の紙　健次郎氏，杉本昌弘博士，菅原真生氏，土岐尚子氏にこの場を借りて深謝致します．本研究は，厚生労働省癌研究助成金，文部科学省グローバルCOEプログラム“*In vivo* ヒト代謝システム生物学”，山形県および鶴岡市の支援によるものである．

文献

1) Ishii, N. et al.：Multiple high-throughput analyses monitor the response of E. coli to perturbations. *Science*, **316**：593-597, 2007.
2) Soga, T. et al.：Quantitative metabolome analysis using capillary electrophoresis mass spectrometry. *J. Proteome Res.*, **2**：488-494, 2003.
3) Sato, S. et al.：Simultaneous determination of the main metabolites in rice leaves using capillary electrophoresis mass spectrometry and capillary electrophoresis diode array detection. *Plant. J.*, **40**：151-163, 2004.
4) Soga, T. et al.：Differential metabolomics reveals ophthalmic acid as an oxidative stress biomarker indicating hepatic glutathione consumption. *J. Biol. Chem.*, **281**：16768-16776, 2006.
5) Hirayama, A. et al.：Quantitative metabolome profiling of colon and stomach cancer microenvironment by capillary electrophoresis time-of-flight mass spectrometry. *Cancer Res.*, **69**：4918-4925, 2009.
6) Warburg, O.：On the origin of cancer cells. *Science*, **123**：309-314, 1956.
7) Kita, K. et al.：Role of complex II in anaerobic respiration of the parasite mitochondria from Ascaris suum and *Plasmodium falciparum*. *Biochim. Biophys. Acta*, **1553**：123-139, 2002.
8) Ullmann, R. et al.：Transport of C(4)-dicarboxylates in Wolinella succinogenes. *J. Bacteriol.*, **182**：5757-5764, 2000.
9) Phang, J.M. et al.：The metabolism of proline, a stress substrate, modulates carcinogenic pathways. *Amino Acids*, **35**：681-690, 2008.
10) Droge, W.：Autophagy and aging-importance of amino acid levels. *Mech. Ageing Dev.*, **125**：161-168, 2004.
11) Mizushima, N. and Klionsky, D.J.：Protein turn-

over via autophagy : implications for metabolism. *Ann. Rev. Nutr.*, **27** : 19–40, 2007.
12) Medina, M. A. et al. : Relevance of glutamine metabolism to tumor cell growth. *Mol. Cell. Biochem.*, **113** : 1–15, 1992.
13) Moreadith, R. W. and Lehninger, A. L. : The pathways of glutamate and glutamine oxidation by tumor cell mitochondria. Role of mitochondrial NAD (P) + -dependent malic enzyme. *J. Biol. Chem.*, **259** : 6215–6221, 1984.
14) Chapman, A. G. et al. : Adenylate energy charge in *Escherichia coli* during growth and starvation. *J. Bacteriol.*, **108** : 1072–1086, 1971.

*　　*　　*

How to 発明 PART 2
全国発明表彰受賞者に聞く

平成21年度 発明協会会長賞
細胞内に存在する数千種類の低分子代謝物の一斉分析が初めて可能に
「メタボローム測定装置」の発明（特許第3341765号）

慶應義塾大学
環境情報学部 先端生命科学研究所 教授
曽我 朋義

1．今回の発明に至った経緯

生命科学では、これまでは謎であった生体や細胞の働きをつまびらかにすることによって、生命を理解し、その成果として人類が直面している健康、食糧、環境、エネルギーなどの問題の解決を目指しています。

生体を構成している細胞は、外界からグルコースなどの栄養源を取り入れ、それを代謝によって他の物質に変換し、活動に必要なエネルギー（ATP）や、アミノ酸、ヌクレオチド、脂質などの低分子化合物（代謝物）を生産しています。細胞には、代謝物が数百から数千種類存在しており、代謝物の総体をメタボロームと呼びます。

細胞の働きはゲノム情報に基づいており、メタボロームはゲノム情報の最終産物です。したがって、細胞の働きを担うゲノム、遺伝子、タンパク質等が変動すれば、最終産物である代謝物にも必然的に変化が生じるため、メタボローム解析によって細胞の状態や振る舞いを把握することができるのです。

近年、急速に発達したメタボローム研究は、代謝調節機構、遺伝子、タンパク質の機能解明といった生命科学の基礎研究に新しい解決策を提供しています。また最近では、疾患の機序解明、バイオマーカーの探索といった医薬分野、機能性成分の探索、ストレスに強い農作物の開発といった食品、農業分野、工業用微生物、バイオ燃料の開発といった工業、環境、エネルギー分野の応用研究にメタボローム研究が幅広く用いられるようになっています。

しかし、私がメタボローム解析に着手した2001年には、メタボローム測定の有用な方法論は存在していませんでした。

細胞には、物理的・化学的性質が非常に似通ったものから全く異なる代謝物が数百から数千種類存在しているため、これらを区別して測定することが極めて困難だったからです。

慶應義塾大学先端生命科学研究所（山形県鶴岡市）のメタボロームプロジェクトに着任した私は、真っ先にメタボローム測定法の開発に取り組みました。

2．技術の概要

測定法を開発するに先立って、細胞内の代謝物の構造を調べると、ほとんどがイオン性の物質でした。最大数万種類の代謝物を一度に測定するには、イオン性物質に対して高分離能を持つキャピラリー電気泳動（CE）と高感度、高選択検出器である質量分析計（MS）を組み合わせたCE-MS法（図１）しかないと直感しました。

実際には、細胞から抽出した代謝物質を、内径が50μm、長さが１mの中空のキャピラリー（毛細管）の一端に注入し、３万Vの電圧をキャピラリーの両端に加えました。図２に示すように、陽イオン性代謝物質は陰極方向に泳動するため、陰極にMSを接続すれば、陽イオン性物質をすべてMSに導入することができます。MSを使い、その代謝物が固有に持つ質量でモニターすることにより、陽イオン性物質を一斉に測定することが可能になりました。反対に、陰イオン性代謝物は陽極方向に泳動するため、陽極にMSを接続することによって陰イオン性代謝物の

一斉分析が可能になりました。

3．技術的課題をどのように克服したか

しかし、CE-MSによるメタボローム測定法の開発は簡単ではありませんでした。当時、CE-MS法では、陰イオンの測定はできないというのが世界の常識でした。

CE-MSで陰イオンを測定すると、数分で電流値が流れなくなりました。最初は、なぜ電流が落ちるのか原因が分かりませんでした。試行錯誤した結果、図3に示すように、陽極側にMSを接続した場合に限り、電流が落ちることに気づきました。

CEで通常使用するフューズドシリカキャピラリーでは、電圧を印加すると、電気浸透流と呼ばれる液流が陽極から陰極方向に発生します（図3－①）。この影響で、数分たつと、キャピラリーの出口（MS側）に空気が入って絶縁されていることが判明しました（図3－②）。

電流が落ちる原因が電気浸透流が陰極方向に発生することだと分かったので、電気浸透流を陽極方向に反転させようと考えました。フューズドシリカキャピラリーの表面にあるシラノールは通常の条件では、H^+が解離して負に帯電します（図3－①）。電圧を印加すると、解離したH^+が陰極に一斉に移動することにより電気浸透流が陰極方向に発生します（図ではH^+は省略）。

電気浸透流を陽極方向に反転させるためには、キャピラリーからOH^-などの陰イオンを解離させる必要があります。そこで、キャピラリーに陽イオン性ポリマーをコーティングしたキャピラリーを試しました。

陽イオン性ポリマーがコーティングキャピラリーでは、OH^-が解離し（キャピラリー表面は正に帯電）、電圧を印加すると、OH^-は一斉に陽極に移動するため電気浸透流が陽極方向に発生するはずです（図3－③、OH^-は省略）。

予想どおり、このキャピラリーを使用することによって、電流が落ちることなく安定した陰イオン性物質の測定が可能になりました。本法が今回、受賞の対象となった発明です。

CE-MSによる陽イオンおよび陰イオンの分析法が完成し、イオン性物質の網羅的な測定が可能になりました。この方法を用いることによって、細胞内に存在する数千種類のイオン性代謝物の一斉分析が可能になり、メタボローム研究は飛躍的に発展しました。私たちは、現在40台のCE-MS装置を保有し（図4）、多くの研究成果が生まれています。

図1　CE-MS装置

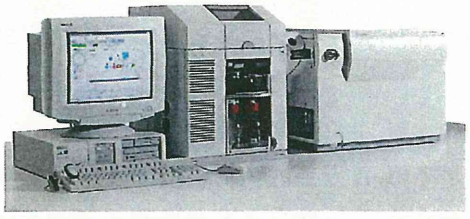

図2　CE-MSの分離の原理

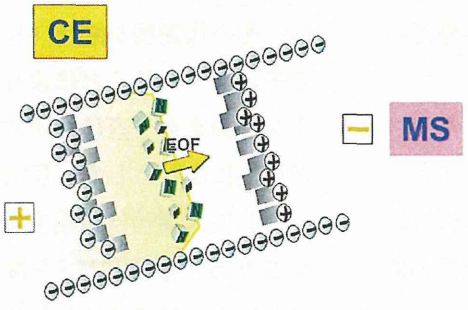

図3　CE-MSによる陰イオン性物質の測定法

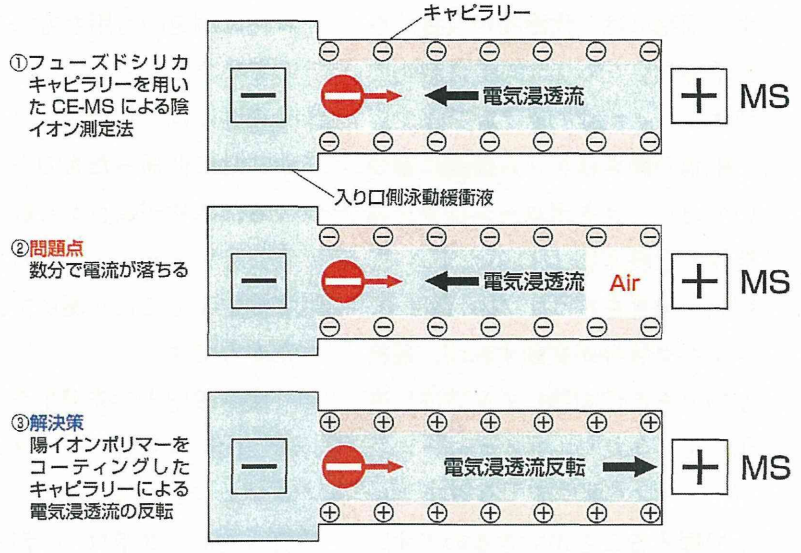

この発明のポイントは2つありました。CE-MSによる陰イオンの測定で電流が流れなくなる原因の究明と、安定した電気浸透流の反転法です。

電流が落ちることなく安定した陰イオンの測定を行うには、陽イオン性物質でコーティングされたキャピラリーを使うしかないという結論に達しましたが、そのような特殊なキャピラリーは市販されていませんでした。

ところが、当時、エーザイにいた石濱泰博士（現・慶應義塾大学先端生命科学研究所准教授）が、こんな物を作ったと私に送ってくれました。それは、まさに私が欲していた陽イオン性のポリマーでコーティングされたキャピラリーでした。

4. 研究・開発の“やりがい”と“心がけ”

いつも思っていることは、研究開発で行う実験が運良く成功しても、得るものは満足感以外何もないということです。実験が成功すると、人は考えることをあまりしません。

しかし、うまくいかないと何が問題だったかを真剣に考えます。仮説が間違っていたのか、実験条件や手順が悪かったのか等々。もし失敗の原因を究明し、解決できれば、それは自分だけの財産となります。

私の経験を振り返ると、自然界は偉大なもので、その実験結果はそうなるべくしてなっています。そのため、実験が思いどおりにならないということは、最初に立てた仮説が間違っている場合がほとんどです。自然界の法則に比べれば、自分の考えはなんて浅薄なのだろうと思い知らされることの連続でした。

これまで多くの研究を行ってきて、実験結果がなぜこうなるのか、分からないことがたくさんありました。しかし、その結果に関して何日も何日もあれこれ悩み考えている時間は結構楽しいものです。また、不思議なもので、朝から晩まで真剣に考えていると、入浴しているときや夢を見ているときに、その答えが思いつくことがあります。

うまくいかない原因が分かり、その問題が解決できたときの爽快感や達成感は、何物にも代えがたいものであり、研究者冥利に尽きます。

図4　慶應義塾大学先端生命科学研究所に並ぶ40台のCE-MSメタボローム測定装置

THE JOURNAL OF BIOLOGICAL CHEMISTRY VOL. 285, NO. 50, pp. 39160–39170, December 10, 2010

Metabolome Analysis Revealed Increase in *S*-Methylcysteine and Phosphatidylisopropanolamine Synthesis upon L-Cysteine Deprivation in the Anaerobic Protozoan Parasite *Entamoeba histolytica*[*] [S]

Received for publication, July 22, 2010, and in revised form, September 23, 2010 Published, JBC Papers in Press, October 5, 2010, DOI 10.1074/jbc.M110.167304

Afzal Husain[‡§1], Dan Sato[¶], Ghulam Jeelani[‡‖2], Fumika Mi-ichi[‡3], Vahab Ali[§4], Makoto Suematsu[‖], Tomoyoshi Soga[¶], and Tomoyoshi Nozaki[‡2,5]

From the [‡]Department of Parasitology, National Institute of Infectious Diseases, 1-23-1 Toyama, Shinjuku-ku, Tokyo 162-8640, Japan, the [§]Department of Parasitology, Gunma University, Graduate School of Medicine, Maebashi 371-8511, Japan, the [¶]Institute for Advanced Biosciences, Keio University, Tsuruoka, Yamagata 997-0052, Japan, and the [‖]Department of Biochemistry and Integrative Medical Biology, School of Medicine, Keio University, Shinjuku, Tokyo 160-8582, Japan

L-Cysteine is ubiquitous in all living organisms and is involved in a variety of functions, including the synthesis of iron-sulfur clusters and glutathione and the regulation of the structure, stability, and catalysis of proteins. In the protozoan parasite *Entamoeba histolytica*, the causative agent of amebiasis, L-cysteine plays an essential role in proliferation, adherence, and defense against oxidative stress; however, the essentiality of this amino acid in the pathways it regulates is not well understood. In the present study, we applied capillary electrophoresis time-of-flight mass spectrometry to quantitate charged metabolites modulated in response to L-cysteine deprivation in *E. histolytica*, which was selected as a model for examining the biological roles of L-cysteine. L-Cysteine deprivation had profound effects on glycolysis, amino acid, and phospholipid metabolism, with sharp decreases in the levels of L-cysteine, L-cystine, and *S*-adenosylmethionine and a dramatic accumulation of *O*-acetylserine and *S*-methylcysteine. We further demonstrated that *S*-methylcysteine is synthesized from methanethiol and *O*-acetylserine by cysteine synthase, which was previously considered to be involved in sulfur-assimilatory L-cysteine biosynthesis. In addition, L-cysteine depletion repressed glycolysis and energy generation, as it reduced acetyl-CoA, ethanol, and the major nucleotide di- and triphosphates, and led to the accumulation of glycolytic intermediates. Interestingly, L-cysteine depletion increased the synthesis of isopropanolamine and phosphatidylisopropanolamine, and it was confirmed that their increment was not a result of oxidative stress but was a specific response to L-cysteine depletion. We also identified a pathway in which isopropanolamine is synthesized from methylglyoxal via aminoacetone. To date, this study represents the first case where L-cysteine deprivation leads to drastic changes in core metabolic pathways, including energy, amino acid, and phospholipid metabolism.

Sulfur-containing amino acids are essential for all living organisms from bacteria to higher eukaryotes and play indispensable roles in various cellular processes, such as methylation and the generation of polyamines, iron-sulfur clusters, and antioxidants. L-Cysteine in particular is essential for the structure, stability, and various protein functions, including catalysis, electron transfer, redox regulation, nitrogen fixation, and sensing for regulatory processes (1).

Entamoeba histolytica is an enteric protozoan parasite that causes hemorrhagic dysentery and extraintestinal abscesses in millions of inhabitants of endemic areas (2). This parasite is generally considered as anaerobic/microaerophilic and has been shown to consume oxygen and tolerate low levels of oxygen pressure but lacks most of the components of antioxidant defense mechanisms, such as catalase, peroxidase, glutathione, and the glutathione-recycling enzymes glutathione peroxidase and glutathione reductase (3, 4). L-Cysteine, which replaces glutathione as a major thiol in *E. histolytica*, is synthesized via a sulfur assimilatory *de novo* cysteine biosynthetic pathway (5–9) that is typically present in bacteria and plants. This pathway consists of two steps that are catalyzed by serine acetyltransferase (SAT, EC 2.3.1.30)[6]

* This work was supported by Grants-in-Aid for Scientific Research 18GS0314, 18050006, and 18073001 (to T. N.) and 20590429 (to D. S.) from the Ministry of Education, Culture, Sports, Science and Technology of Japan, Grant H20-Shinkosaiko-016 for research on emerging and re-emerging infectious diseases from the Ministry of Health, Labour and Welfare of Japan, and a grant for research to promote the development of anti-AIDS pharmaceuticals from the Japan Health Sciences Foundation (to T. N.).

[S] The on-line version of this article (available at http://www.jbc.org) contains supplemental Fig. S1.

[1] Supported by the Monbukagakusho Scholarship from the Ministry of Education, Culture, Sports, Science and Technology.

[2] Supported by the Global Center of Excellence Program for Human Metabolomic System Biology of the Ministry of Education Culture, Sports, Science and Technology.

[3] Present address: Division of Molecular and Cellular Immunoscience, Dept. of Biomolecular Sciences, Saga University, Saga 849-8581, Japan.

[4] Present address: Dept. of Biochemistry, Rajendra Memorial Research Institute of Medical Sciences, Agamkuan, Patna-800007, India.

[5] To whom correspondence should be addressed: Dept. of Parasitology, National Institute of Infectious Diseases, 1-23-1 Toyama, Shinjuku-ku, Tokyo 162-8640, Japan. Tel.: 81-3-5285-1111, Ext. 2600; Fax: 81-3-5285-1219; E-mail: nozaki@nih.go.jp.

[6] The abbreviations used are: SAT, serine acetyltransferase; CS, cysteine synthase; CE-TOFMS, capillary electrophoresis time-of-flight mass spectrometry; 2′,7′-DCF-DA, 2′,7′-dichlorodihydrofluorescein di-acetate; ESI, electrospray ionization; Cho, choline; Cho-P, choline phosphate; OAS, *O*-acetylserine; SMC, *S*-methylcysteine; SAM, *S*-adenosylmethionine; Ispn, isopropanolamine; Ispn-P, isopropanolamine phosphate; PtdIspn, phosphatidylisopropanolamine; Etn, ethanolamine; Etn-P, ethanolamine phosphate; PtdEtn, phosphatidylethanolamine.

(7, 8) and cysteine synthase (CS; OAS (thiol) lyase; EC 4.2.99.8) (5). In addition to the presence of prokaryotic/plant-like L-cysteine biosynthesis, *E. histolytica* is also unique because the forward and reverse trans-sulfuration pathways are absent and interrupted, respectively. Furthermore, through lateral gene transfer from archaea, *E. histolytica* has acquired methionine γ-lyase (EC 4.4.1.11), an enzyme that degrades L-methionine, L-homocysteine, and L-cysteine (10–12). Thus, although typical parasitic protists show degenerated amino acid metabolic pathways, particularly those associated with catabolism, because of the parasitic lifestyle, sulfur-containing amino acid metabolism appears to have uniquely evolved in *E. histolytica.* However, the specific role of this pathway in this organism remains unclear.

L-Cysteine is the principal low molecular weight thiol in *E. histolytica* and is involved in the survival, growth, attachment, elongation, motility, gene regulation, and antioxidative stress defense of this organism (13–17). Because sulfur-containing amino acid metabolism differs significantly between *E. histolytica* and its mammalian host, the molecular dissection and characterization of this pathway may lead to the development of new chemotherapeutics against this parasite (18).

Here, to gain further insight into the roles and regulatory mechanisms of sulfur-containing amino acid metabolism and individual metabolites in *E. histolytica*, we utilized capillary electrophoresis time-of-flight mass spectrometry (CE-TOFMS) (19–21) for the metabolomic profiling of this parasite. We observed drastic changes in the metabolome as a result of L-cysteine depletion, which led to the discovery of novel L-cysteine-mediated regulation of several metabolic pathways in *E. histolytica.*

EXPERIMENTAL PROCEDURES

Chemicals and Reagents—All of the chemicals of analytical grade were purchased from either Wako or Sigma-Aldrich unless otherwise mentioned. 2′,7′-Dichlorodihydrofluorescein di-acetate (2′,7′-DCF-DA) was purchased from Invitrogen. 1-Aminoacetone hydrochloride was obtained from United States Biologicals. High performance thin layer chromatography silica gel 60 plates were purchased from Merck. [U-$^{13}C_5$,^{15}N]L-Methionine and [U-$^{13}C_3$,^{15}N]L-serine were purchased from Cambridge Isotope Laboratories. Stock solutions of metabolite standards (1–100 mmol/liter) for CE-MS analysis were prepared in either Milli-Q water, 0.1 mol/liter HCl, or 0.1 mol/liter NaOH. A mixed solution of the standards was prepared by diluting stock solutions with Milli-Q water immediately before CE-TOFMS analysis.

Microorganisms and Cultivation—Trophozoites of the *E. histolytica* clonal strain HM-1: IMSS cl 6 were maintained axenically in Diamond's BI-S-33 medium at 35.5 °C, as described previously (22, 23). Trophozoites were harvested in the late logarithmic growth phase 2–3 days after the inoculation of medium with one-thirtieth to one-twelfth of the total culture volume.

Metabolic Labeling and Metabolite Extraction—*E. histolytica* trophozoites were cultivated in either standard BI-S-33 medium containing 8 mM L-cysteine or L-cysteine-deprived medium for 48 h. For the metabolic labeling, trophozoites were cultured in the presence of either 3 mM stable isotope-labeled [U-$^{13}C_5$,^{15}N]L-methionine or 6 mM [U-$^{13}C_3$,^{15}N]L-serine in L-cysteine-deprived medium for 48 h as described above. To extract metabolites, ~1.5 × 10^6 cells from each condition were harvested and washed twice with 5% mannitol. The cells were then suspended in 1.6 ml of methanol containing 16 μM of each internal standard, 2-(*N*-morpholino)ethanesulfonic acid, methionine sulfone, and D-camphor-10-sulfonic acid and mixed with 1.6 ml of chloroform and 640 μl of deionized water. After vortexing, the mixture was centrifuged at 4,600 × *g* at 4 °C for 5 min. The aqueous layer (1.6 ml) was filtrated using an Amicon Ultrafree-MC ultrafilter (Millipore Co.) and centrifuged at 9,100 × *g* at 4 °C for ~2 h. The filtrate was dried and preserved at −80 °C until mass spectrometric analysis (24). Prior to the analysis, the sample was dissolved in 20 μl of deionized water containing reference compounds (200 μmol/liter each of 3-aminopyrrolidine and trimesic acid).

Instrumentation and CE-TOFMS Conditions—CE-TOFMS was performed using an Agilent CE capillary electrophoresis system equipped with an Agilent 6210 time-of-flight mass spectrometer, Agilent 1100 isocratic HPLC pump, Agilent G1603A CE-MS adapter kit, and Agilent G1607A CE-ESI-MS sprayer kit (Agilent Technologies, Waldbronn, Germany). The system was controlled by Agilent G2201AA ChemStation software for CE. Data acquisition was performed by Analyst QS software for Agilent TOF (Applied Biosystems and MDS Sciex).

CE-TOFMS Conditions for Cationic Metabolite Analysis—Cationic metabolites were separated in a fused silica capillary (50-μm inner diameter × 100-cm) filled with 1 mol/liter formic acid as the reference electrolyte (25). Sample solution (~3 nl) was injected at 50 mbar for 3 s, and a positive voltage of 30 kV was applied. The capillary and sample trays were maintained at 20 °C and below 5 °C, respectively. Sheath liquid composed of methanol/water (50% v/v) that contained 0.1 μmol/liter hexakis (2,2-difluorothoxy)phosphazene was delivered at 10 μl/min. ESI-TOFMS was operated in the positive ion mode. The capillary voltage was set at 4 kV, and a flow rate of nitrogen gas (heater temperature, 300 °C) was set at 10 p.s.i. For TOFMS, the fragmenter voltage, skimmer voltage, and octapole radio frequency voltage (Oct RFV) were set at 75, 50, and 125 V, respectively. An automatic recalibration function was performed using two reference masses of reference standards; protonated [^{13}C]methanol dimer (*m/z* 66.063061) and protonated hexakis (2,2-difluorothoxy)phosphazene (*m/z* 622.028963), which provided the lock mass for exact mass measurements. Exact mass data were acquired at the rate of 1.5 cycles/s over a 50–1,000 *m/z* range.

CE-TOFMS Conditions for Anionic Metabolite Analysis—Anionic metabolites were separated in a cationic polymer-coated COSMO(+) capillary (50-μm inner diameter × 110-cm) (Nacalai Tesque) filled with 50 mmol/liter ammonium acetate solution, pH 8.5, as the reference electrolyte (26, 27). Sample solution (~30 nl) was injected at 50 mbar for 30 s, and a negative voltage of −30 kV was applied. Ammonium acetate (5 mmol/liter) in methanol/water (50% v/v) that contained 0.1 μmol/liter hexakis (2,2-difluorothoxy)phosphazene was delivered as sheath liquid at 10 μl/min. ESI-TOFMS was operated

in the negative ion mode. The capillary voltage was set at 3.5 kV. For TOFMS, the fragmenter voltage, skimmer voltage, and Oct RFV were set at 100, 50, and 200 V, respectively (27). An automatic recalibration function was performed using two reference masses of reference standards: deprotonated ^{13}C acetate dimer (*m/z* 120.038339) and acetate adduct of hexakis (2,2-difluorothoxy)phosphazene (*m/z* 680.035541). The other conditions were identical to those used for the cationic metabolite analysis.

CE-TOFMS Data Processing—Raw data were processed using the in-house software Masterhands (28). The overall data processing flow consisted of the following steps: noise filtering, baseline removal, migration time correction, peak detection, and integration of peak area from a 0.02 *m/z*-wide slice of the electropherograms. This process resembled the strategies employed in widely used data processing software for LC-MS and GC-MS data analysis, such as MassHunter (Agilent Technologies) and XCMS (29). Subsequently, accurate *m/z* values for each peak were calculated by Gaussian curve fitting in the *m/z* domain, and migration times were normalized using alignment algorithms based on dynamic programming (19, 30). All of the target metabolites were identified by matching their *m/z* values and normalized migration times with those of standard compounds in the in-house library.

Quantitation of Reactive Oxygen Species—Fluorescence spectrophotometry was used to measure the production of intracellular reactive oxygen species using 2′,7′-DCF-DA as a probe as previously described (31). Briefly, *E. histolytica* cells were washed in PBS, and 5.0×10^5 cells were then incubated in 1 ml of PBS containing 20 μM 2′,7′-DCF-DA for 30 min at 35.5 °C in the dark. The intensity of fluorescence was immediately read at excitation and emission wavelengths of 492 and 519 nm, respectively.

L-Cysteine/SMC Synthase Assay—L-Cysteine/SMC synthase was assayed by measuring acetate production through the coupling reaction of this enzyme with acetate kinase, pyruvate kinase, and lactate dehydrogenase. Acetate kinase generates ADP and acetyl-phosphate from acetate and ATP. The ADP production was coupled with the oxidation of NADH (ϵ_{340} = 6.22 mM^{-1} cm^{-1}) through pyruvate kinase and lactate dehydrogenase (32). The standard reaction mixture contained 50 mM of Tris-Cl, pH 8.0, 3 mM OAS, 3 mM sodium sulfide or sodium methanethiolate, 4 units each of acetate kinase, pyruvate kinase, and lactate dehydrogenase, 0.5 mM ATP, 0.3 mM NADH, and 1–2 μg of recombinant cysteine synthase. The reactions were initiated by the addition of recombinant cysteine synthase, and optical absorbance was read at 340 nm on a Shimadzu spectrophotometer. Kinetic parameters were determined using various concentrations (0.1–6 mM) of sodium sulfide, sodium methanethiolate, and OAS. The kinetic parameters were estimated using the nonlinear regression function obtained from the GraphPad Prism software (GraphPad Software Inc., San Diego, CA).

Choline and Ethanol Quantitation—The amount of choline (Cho) in the metabolite extracts was quantitated enzymatically using components of the Amplex® Red sphingomyelinase assay kit (Invitrogen). Briefly, Cho was first oxidized by Cho oxidase to betaine and hydrogen peroxide. The produced hydrogen peroxide was then reacted with Amplex® Red reagent in a 1:1 stoichiometry in the presence of horseradish peroxidase to generate the highly fluorescent product resorufin, which was read in a fluorescence spectrophotometer (model F-2500; Hitachi) at excitation and emission wavelengths of 545 and 590 nm, respectively. Ethanol production by trophozoites cultured in either normal or L-cysteine-deprived medium was determined as described previously (33).

Extraction of Lipids, Thin Layer Chromatography, and Phospholipid Quantitation—Cells cultured in either normal or cysteine-deprived medium for 48 h were collected by centrifugation, and lipids were then extracted by the Bligh and Dyer's method (34). The extracted lipids were analyzed by two-dimensional high performance thin layer chromatography using a solvent system of chloroform:methanol:28% ammonium hydroxide (65:25:5 v/v/v) in the first direction and chloroform:acetone:methanol:Acetic acid:water (50:20:10:10:5 v/v/v/v/v) in the second. The phosphorus content of phospholipids was determined after scraping representative spots from the plate, as described previously (35). The lipids were visualized by exposing TLC plates to iodine vapor.

RESULTS

L-Cysteine Deprivation Caused Accumulation of O-Acetylserine and S-Methylcysteine—We first verified that L-cysteine deprivation affected intracellular L-cysteine/L-cystine concentrations in *E. histolytica*. Under normal culture conditions (8 mM L-cysteine), the intracellular concentrations of L-cysteine and L-cystine were 431 ± 52 and 202 ± 40 pmol, respectively, per 2×10^5 cells. Approximately two-thirds (68 ± 7%) of L-cysteine/L-cystine was present in a reduced form, whereas the remaining third was present in an oxidized form. Upon L-cysteine deprivation for 48 h, both L-cysteine and L-cystine decreased to nearly undetectable levels (88 ± 11 and 79 ± 10% decrement, respectively) (Fig. 1*A*). These results suggest that the intracellular L-cysteine/L-cystine concentrations in *E. histolytica* are greatly affected by the composition of the extracellular milieu.

We also examined whether oxidative stress induced by paraquat affected intracellular L-cysteine/L-cystine concentrations. Treatment of the amebae with 2 mM paraquat for 10 h led to 60.6 ± 8.8 and 41.4 ± 7.3% decreases in the levels of L-cysteine and L-cystine, respectively. Under conditions of L-cysteine limitation, the intracellular levels of reactive oxygen species increased by >4-fold, which was comparable with the 3.3-fold increase observed in paraquat/air-treated cells (Fig. 1*B*). These results suggest that L-cysteine may be an important scavenger of reactive oxygen species in *E. histolytica.*

Among the ~90 intermediary metabolites that were measured by CE-TOFMS-based metabolomic analysis, which include amino acids, organic acids, and nucleotides (19–21), L-cysteine depletion caused drastic changes in the metabolites of *E. histolytica* involved in sulfur-containing amino acid metabolism (Fig. 1*C*). L-Cysteine depletion resulted in a sharp increase in *O*-acetylserine (OAS) (nearly undetectable under normal conditions), an activated form of L-serine that is synthesized from L-serine and acetyl-CoA by SAT. We also ob-